Article

Statistical Analysis of LEO and GEO Satellite Anomalies and Space Radiation

Jeimmy Nataly Buitrago-Leiva [1,*], Mohamed El Khayati Ramouz [1], Adriano Camps [1,2,3] and Joan A. Ruiz-de-Azua [4]

1   CommSensLab-UPC, Department of Signal Theory and Communications, Universitat Politècnica de Catalunya, Carrer de Jordi Girona 31, 08034 Barcelona, Spain; mohamed.el.khayati@upc.edu (M.E.K.R.); adriano.jose.camps@upc.edu (A.C.)
2   Institut d'Estudis Espacials de Catalunya IEEC, Parc Mediterrani de la Tecnologia (PMT), Campus del Baix Llobregat, UPC, 08860 Barcelona, Spain
3   College of Engineering, United Arab Emirates University, Al Ain P.O. Box 15551, United Arab Emirates
4   Space Communications Research Group, i2CAT Fundation, Carrer del Gran Capità, 2, 08034 Barcelona, Spain; joan.ruizdeazua@i2cat.net
*   Correspondence: jeimmy.nataly.buitrago@upc.edu

Abstract: Exposure to space radiation substantially degrades satellite systems, provoking severe partial or, in some extreme cases, total failures. Electrostatic discharges (ESD), single event latch-up (SEL), and single event upsets (SEU) are among the most frequent causes of those reported satellite anomalies. The impact of space radiation dose on satellite equipment has been studied in-depth. This study conducts a statistical analysis to explore the relationships between low-Earth orbit (LEO) and geostationary orbit (GEO) satellite anomalies and particle concentrations, solar and geomagnetic activity in the period 2010–2022. Through a monthly and daily timescale analysis, the present work explores the temporal response of space disturbances on satellite systems and the periods when satellites are vulnerable to those disturbances.

Keywords: satellite anomalies; space radiation; solar activity; geomagnetic disturbances

1. Introduction

Besides the technical specifications and the fulfillment of functional capabilities of electronic components, their durability and resilience in space conditions are a major concern for the space industry. Over time, substantial evidence has been accumulated relating an significant number of satellite anomalies to space environment conditions. For example, in the Telastra database [1], which lists over 1500 anomalies primarily associated with GEO satellites, samples that reported failures suspected to be related to radiation effects are TDRS-1 in 1983, TDF-1 in 1989, Telecom 2A in 1994, and Thaicom-5 in 2011. More satellite failures associated to space weather have been reported in several studies, such as [2–7]. Thus, understanding the space environment's effects is essential to advance towards more robust designs and operational strategies [8,9].

In this regard, several studies, mostly based on statistical analysis and primarily focused on GEO anomalies [10,11], have been carried out to figure out the temporal response of space disturbances on satellite equipment, the most susceptible periods by which the anomaly rate increases, and the effects of the different radiation particles upon several systems. For instance, [12] analyzed 95 commercial satellite anomalies in 1997–2009, obtaining a strong correlation between anomaly rate and geomagnetic activity, and interesting seasonal variations in the occurrence of GEO anomalies. Similarly, [13] investigated potential statistical correlations between electron/proton flux data and GEO satellite anomalies for the period 1986–1994, showing the susceptibility of GEO satellites to solar protons during solar maximum activity, and relativistic electrons during the minimum activity.

However, the majority of research, including the aforementioned studies, consider only GEO anomalies in their analysis, which restricts our understanding to high orbits only. In addition, according to authors' knowledge, no similar analysis has been performed for anomalies that occurred in the last years, to evaluate the effectiveness and evolution of radiation hardened (RadHard) components. Furthermore, considering the "New Space Era" from 2013 onwards, and the revolution towards small satellites (e.g., CubeSats) [14], it is critical to understand how the minimization of satellite mechanical structure and electronic components mitigates radiation exposure [15,16]. In that regard, this study presents a statistical analysis that compares reported anomalies of LEO ($\leq$1000 kg) and GEO satellites ($\leq$5000 kg) spanning the period from 2010 to 2022 with four variables: sunspot number (SSN), coronal mass ejections (CMEs), Kp-index, and the disturbance storm-time (Dst) index. Moreover, it investigates the connection between satellite anomalies and the flux of protons, electrons, and X-ray particles. In particular, this study aims to: (1) understand the temporal response of space weather disturbances and satellite anomalies occurrence; (2) ascertain how solar and geomagnetic storms affect satellites based on their orbit, thus, LEO and GEO anomalies are analyzed separately; (3) identify susceptible periods of time when the anomaly rate fluctuates significantly; (4) determine the most suitable timescale to evaluate anomalies and space weather depending on the orbit and disturbance indicator; and (5) examine the effects that particle fluxes have on satellite systems.

This manuscript is organized as follows: space radiation characteristics and their potential impact on satellite systems are briefly introduced in Section 2. Section 3 describes the anomalies databases, the space radiation indicators used, and the methodology followed to carry out the analysis. Section 4 presents the results of the statistical analysis, while in Section 5 the results are discussed and summarized.

2. Space Weather Effects on Satellite Systems

Space weather phenomena and their related particle properties can affect different satellite systems. The primary sources of radiation in Earth's satellite orbits proceed from solar particle events (SPEs), galactic cosmic rays (GCR), and auroral particles (mostly low-energy electrons) [17]. High-energy charged particles known as GCRs originate outside the solar system and are composed of protons, electrons, and heavy ions. GCR and solar activity have a negative correlation, which means that, when solar activity is at its lowest and the Sun's magnetic field is weaker, more GCRs enter into the inner solar system [18]. As for solar radiation, SPEs occur when charged particles in the Sun's atmosphere are accelerated at very high velocities, escaping to the interplanetary space [19,20]. In case those particles have enough energy to penetrate the Earth's magnetic field, they reach the Earth's magnetosphere and ionosphere surrounding mainly the North and South poles. SPEs have a mean composition of 96.4% protons, 3.5% alpha particles, and 0.1% heavier ions [21], where the peak flow of particles with energies above 10 MeV per nucleon can surpass 10^5 cm^{-2}s^{-1} [22].

The radiation intensity that a satellite may encounter during its lifetime depends significantly on its orbit altitude and inclination [23]. For example, orbits with low altitudes are often attained by less radiation flow due to the shielding effects of Earth's magnetic field and atmosphere thus, providing better safety for LEO satellites [23–25]. However, in LEO, satellites that, for example, orbit across the inner Van Allen belt, where the Earth's magnetic field traps the high-energy protons, will still be substantially exposed to high dosages [26–28]. In addition, the radiation in orbit also varies depending on the temporal fluctuations of several space phenomena such as the solar cycles, solar flares, solar wind, and geomagnetic storms. Hence, the satellite subsystems may experience a variety of effects and disruptions based on the particles' characteristics (e.g., typology, energy levels) derived from those space weather events (see Figure 1) [29,30]. The main radiation effects on satellite systems, as well as those particles causing them, can be summarized in the following points:

- Surface charging of satellite: Caused by low-energy electrons (<100 keV), observed typically in the inner magnetosphere during geomagnetic storms [12].
- Satellite internal electrostatic discharge: Caused by high-energy electrons (>100 keV), observed in Earth's dynamic outer radiation belt.
- Single event effects: Caused by high-energy protons (>10 MeV) and heavier ions, derived from solar flares, and coronal mass ejections (CMEs).
- Total dose effects: Caused by cumulative charged protons and electrons derived from several space weather events.
- Others: Other effects such as those related to communications and attitude control failures, due to magnetic field variations, and ionospheric anomalies, among others [31].
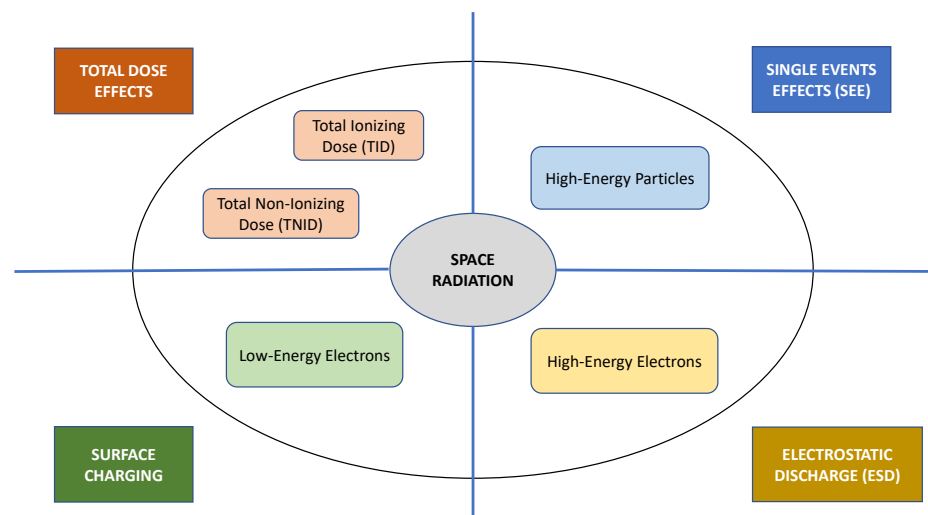

Figure 1. Radiation particles and their effects on satellite systems.

Although satellites are conceived to operate in the space environment, some particles can interact with the satellites' surfaces and damage the electronics, creating serious damage to the system [32,33]. Within this context, numerous subsystems and equipment in the satellite are significantly vulnerable to radiation effects [33]. For instance, solar arrays are susceptible to ultraviolet (UV) radiation, polymers are vulnerable to high-energy photons [34], and high-energy electrons may provoke severe electrical discharges. In addition, high-energy protons and ions can substantially affect sensitive electronic components by changing bits (SEU) and disabling device capabilities (single-event Latchup or Burnout, SEL or SEB, respectively) [35–37].

3. Data and Methods

3.1. LEO and GEO Satellite Anomalies

Anomalies associated with GEO satellites have been extracted from the Seradata database [38]. Regarding anomalies corresponding to LEO orbit, besides those reported in Seradata [38], additional LEO anomalies reported in the Gunter Space Page, eoPortal [39], and NASA [40] have been assembled in a custom database. Only those anomalies that occurred from 1 January 2010 to 31 December 2022, have been considered, regardless of the satellite's launch year. In addition, to remove any potential outliers that may introduce bias and influence the results, several filters have been introduced in the databases. In particular:

1. Anomalies lacking a clear specification of the month and day of occurrence in their description were discarded, given the significance of the anomalies' date in the analysis.
2. Launch failures were removed as their occurrence is typically attributed to mechanical or procedural errors unrelated to space radiation.

3. Unless the cause of the specified anomaly is closely related to radiation effects (e.g., ESD), failures occurring within the first month after launch were excluded, as they may be due to "infancy failures" [41] or lack of testing processes.

4. Anomalies whose cause is not exclusively attributable to radiation effects are discarded. Clear examples are those anomalies related to specific mechanical failures (e.g., related to antenna and solar panel deployment), propulsion systems (e.g., fuel loss), and data misinterpretation by operators, among others.

5. Only one anomaly—the first failure, if specified—is taken into consideration for satellites that have multiple reported failures in a single day. Thus, anomalies that can be derived from the malfunctioning of the initial one are removed.

Thus, considering these defined filters, 518 and 511 anomalies of LEO and GEO satellites, respectively, are considered in the analysis (see Figure 2).
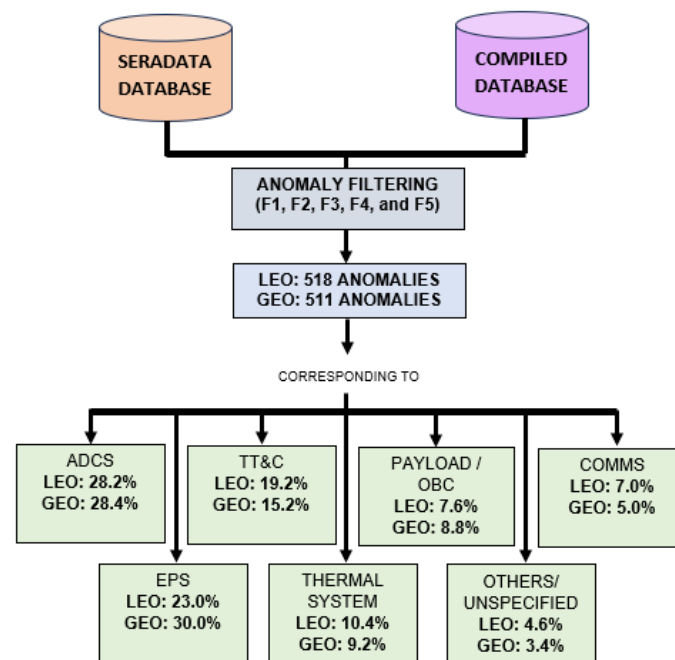

Figure 2. Anomaly selection criteria and their categorization per subsystem. F1, F2, F3 F4, and F5 corresponds to the filters described in Section 3.1.

3.2. Space Radiation Indicators

On one hand, the Sun does provide most of the particle flow reaching the Earth. However, its low magnetic field during minimal SSN facilitates GCR access to the solar system. On the other hand, Earth's magnetic field is crucial to shield or trap radiation particles that can affect satellite missions. Thus, the solar cycle and geomagnetic activity play a fundamental role in the Earth's orbit radiation density and appear to be the most convenient radiation and perturbation indicators. In this regard, and following previous research [6,12,42,43], the SSN, Kp, CME speed, and Dst indices have been considered in this analysis.

Sunspots are regions on the Sun's surface cooler than others, where the magnetic fields are so extremely strong that they keep some of the heat within the Sun from reaching the surface. The magnetic field lines near sunspots often tangle and cross, causing energy explosions and releasing a lot of radiation into space. Those explosions, also known as solar flares, are sometimes accompanied by huge bubbles of radiation and particles from the Sun that explode into space at very high speeds when the Sun's magnetic field lines suddenly reorganize [44]. Thus, sunspots are closely linked to solar activity, resulting in an important indicator to identify and interpret satellite anomalies. Sunspot data have been

obtained from the Royal Observatory of Belgium website [45,46], which provides daily sunspot activity from 1 January 1818 onwards.

CMEs consist of the expulsion of a vast amount of plasma from the solar corona into space at speeds reaching thousands of kilometers per second. Primarily composed of electrons and protons, these ejections also contain traces of helium, oxygen, and iron in ion form [47]. This flow of radiation, when detached from the Sun, poses a significant risk when directed towards Earth [48]. If its magnetic field is oriented southward, it could cause significant damage to electrical circuits, transformers, and communication systems, as well as affect the Earth's magnetic field for a period [49]. CMEs are characterized by parameters such as the date and time of their appearance in the field of view (FOV) of the LASCO/C2 telescope and the central position angle (CPA), the latter being crucial for distinguishing between multiple simultaneous CMEs. CMEs with an apparent width of 360 degrees are marked as Halo and can be symmetric (S) or asymmetric, with brightness asymmetry (BA) or outline asymmetry (OA). Additionally, they are defined by three speeds, linear, quadratic evaluated at the time of the last measurement, and quadratic at 20 solar radii, as well as by their acceleration, which can be positive, negative, or close to zero. The mass of a CME, taken as a representative when it reaches a quasi-constant value after increasing in the first few solar radii, along with the linear speed, allows for the calculation of its kinetic energy [50]. However, given that the linear velocity parameter of CMEs refers to the speed at which material ejected from the Sun moves into space, this study used this parameter as a relevant comparison metric to determine the speed at which this material moves in a straight line away from the Sun. This is an essential element because it can alter how CMEs interact with the Earth's magnetosphere, thereby influencing space weather. Thus, CMEs' linear velocity data during the study period were extracted from the NASA SOHO LASCO CMEs Catalog, Version 2 [50]. This catalog categorizes all daily CMEs records collected by the ESA/NASA SOHO satellite, dedicated to solar observation. The main instrument used, called LASCO, enables the observation of the solar corona [51]. In this analysis, the authors utilized the CME speed index, which is defined as the highest linear speed recorded for each day [52].

Regarding the geomagnetic activity, two variables have been used. The first one, the K-index, also known as the planetary K-index, is an indicator that quantifies the disturbances in the horizontal component of the Earth's magnetic field with an integer between 0 and 9, with 1 indicating low magnetic activity and 5 or more indicating a geomagnetic storm [11,53]. The Kp-index, which is updated every three hours, is calculated by averaging the K-indices from a network of thirteen geomagnetic observatories located in mid-latitude regions. As sunspots data, the Kp-index has been acquired from the Royal Observatory of Belgium website [45,46], covering daily Kp-index information from 1 January 2009 onwards. As for the second indicator, unlike the Kp-index, which offers general information about the geomagnetic activity, the Dst index assesses disturbances in the Earth's magnetic field induced by geomagnetic storms [54]. A higher negative value of the Dst index indicates more severe geomagnetic disruptions [55]. This could be due to high solar activity, such as solar flares or CMEs, which produce stronger solar winds, and hence cause greater disruption in the Earth's magnetic field [56]. Whereas the Kp-index provides a comprehensive assessment of geomagnetic activity on Earth, the Dst index differs by especially targeting disturbances induced by geomagnetic storms. The Dst data have been obtained from the geomagnetic equatorial Dst index Home Page, providing information dating back to 1953 [57].

As mentioned before, the solar corona is primarily composed of plasma, an atmosphere of ionized gas that is not static and can even detach from the star [58]. This movement of the corona is known as solar wind, a stream of charged particles released from the Sun's upper atmosphere. This plasma consists mainly of electrons, protons, and alpha particles, with thermal energies ranging from 1.5 to 10 eV [59]. To assess the risk that particle fluxes pose to Earth, especially in a satellite environment, this study also assesses the effects that several particle fluxes such as protons, electrons, and X-rays can have upon

satellite equipment. The corresponding data were extracted from weekly reports in the historical repository of the National Oceanic and Atmospheric Administration's Space Weather Prediction Center (NOAA), provided by the GOES-14 and GOES-15 satellites from 1 January 2010 to 31 December 2022 [60,61]. For the analysis, protons with energies larger than 10 MeV (proton fluence - protons/cm²-day-steradian) and electrons with energies of more than 2 MeV (electron fluence - electrons/cm^2-day-steradian) were considered based on established criteria and literature regarding known radiation effects on satellite systems [62,63]. For the X-ray analysis, the weekly report from NOAA was also utilized, specifically the section on daily solar data: X-ray background flux, identified by a letter indicating the level of solar flare activity: A (between 10^{-8} and 10^{-7} W/m^2), B (between 10^{-7} and 10^{-6} W/m^2), and C (between 10^{-6} and 10^{-5} W/m^2). Within these ranges, a numerical value is used to specify the flux measured in watts per square meter [64].

Satellite anomalies have been correlated with space weather indicators at several timescales. Initially, a monthly time series has been conducted over thirteen years to provide a general overview and to evaluate potential trends associated with solar cycle phases. Afterward, months have been classified based on the number of anomalies that occurred in their course, and compared with the space weather indicators considered. In addition, aiming to capture anomalies that may have been caused by radiation accumulation, not only those months in which anomalies were reported, but also the mean SSN, Kp, CME speed, and Dst indices of the three months before were assessed. In order to determine any anomaly patterns between the seasons, the next step consisted of computing the mean anomaly and space radiation indicators of each month of the year.

Considering that solar wind plasma reaches the Earth in 3–4 days, and plasma emitted by other active events such as solar flares and CMEs in even less time, a daily analysis has been carried out by comparing the space weather events and particle density to anomalies reported. The analysis contrasts the average space weather conditions of days exhibiting three or more anomalies with days with no anomalies reported. As proposed for the monthly analysis, the analysis is conducted not only for the selected individual days, but also for the preceding seven days.

4. Results

4.1. Monthly Analysis

Figure 3 presents the relationship between the space weather variables and satellite in-orbit anomalies. Regarding solar activity, it can be seen that in some periods, when solar activity is high, the number of anomalies also rises considerably. For the GEO case, this can be seen in periods such as September 2011–December 2011, January 2014–April 2014, and May 2022–August 2022, whereas for LEO, this effect is seen from September 2021 to April 2022, corresponding to a significant increase in anomalies, from which most correspond to reported Starlink satellites failures [65]. Nevertheless, there are also some periods in which the anomaly rate increases when solar activity is low, such as September 2019–December 2019 and April 2019–August 2019 for GEO and LEO orbit, respectively. This lack of correlation during low solar activity has prevented several studies from establishing any clear relationship between satellite failures and solar activity [12]. Several studies, such as [13], when investigating the link between solar activity and GEO anomalies from 1986–1994, have obtained similar relations, concluding that most satellite failures during maximum solar activity are caused by high solar protons events [23]. However, when the SSN is low and thus the solar proton fluxes are minimal, satellite anomalies are mostly due to relativistic electron fluxes, which tend to be maximal.

As for the geomagnetic activity, GEO and LEO anomalies do present correlation patterns in those months when geomagnetic activity slightly increases (high Kp-index and low Dst index), such as January 2012–April 2012, January 2014–April 2014, and September 2019–December 2019 for GEO, and April 2011–August 2011 and January 2022–April 2022 in LEO anomalies. However, in some months, even having a low magnetic activity, the number of anomalies rises (e.g., September 2012–December 2012 for GEO, and May 2014–August 2014

for LEO). Nevertheless, several cases also show that substantial solar and magnetic activity happens in the months before the anomaly occurrence, rather than within that particular month. This is consistent, considering that, after an injection of charged particles, they can remain on satellite orbits afterward. Hence, the effects of this radiation on satellite equipment may be not necessarily when the space weather indicators reach their peak, and failures may occur in the upcoming days, weeks, or months. Therefore, it is crucial to consider a time lag, and temporally extend the analysis by including space environment characteristics of the period before the anomalous occurrence month.
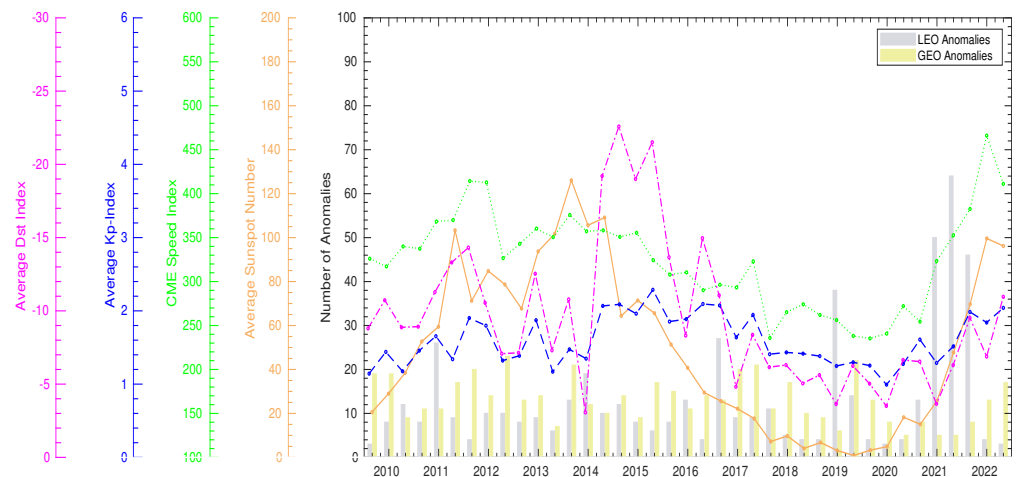

Figure 3. LEO/GEO satellites' anomalies and solar and geomagnetic activity correlation (2010–2022). Sunspot number and CME speed index are used to quantify solar activity, whereas Kp and Dst indices are used to quantify geomagnetic activity. Despite using a monthly timescale for analysis, this figure is plotted by grouping four months for visual simplicity.

Thus, every month, from January 2010 to December 2022, has been categorized depending on the number of anomalies that occurred in that month. Then, each group was compared to the average SSN, Kp, CME speed, and Dst indices of the anomaly event month and three prior months to understand the temporal response of satellite equipment due to space environment variations (see Figure 4). Therefore, all months having anomalies within a range have had their SSN, Kp, CME speed, and Dst indices averaged to calculate the mean SSN, Kp, CME speed, and Dst indices of that group.

In the case of GEO anomalies, the average SSN for those months over three anomalies increase significantly (from 40 to 70 sunspots/month), not only for the month in which the anomaly occurs, but also for the three prior months. This suggests that, rather than relativistic electrons, most of the considered anomalies may be caused by solar proton events during maximum solar activity. Furthermore, previous months (M-1, M-2, M-3) do show even higher solar activity regarding the month in which the failures happened for those months between 3–5 and over 10 anomalies, which may indicate that the temporal response of space conditions on the equipment may not necessarily be instantaneous (Figure 4e). Nonetheless, none of these trends are clearly visible for the examined LEO anomalies (Figure 4a). Concerning CMEs, as for LEO and GEO, the average CME speed index for months presenting $6 \leq A_M \leq 9$ and $A_M \geq 10$ is slightly higher (reaching 340 km/s) than for months with a low anomaly rate. Similarly, considering that CMEs can also cause geomagnetic storms, months with more than ten GEO anomalies show a marginally higher Kp index in the anomaly month (M) as well as reductions for the preceding months. On the other hand, months with anomalies between six and nine also show a lower Dst index, particularly in the month preceding the anomaly occurrence (M-1) (Figure 4g,h). Similarly to those trends observed with SSN, those geomagnetic patterns are not very apparent with the LEO anomalies (Figure 4c,d).
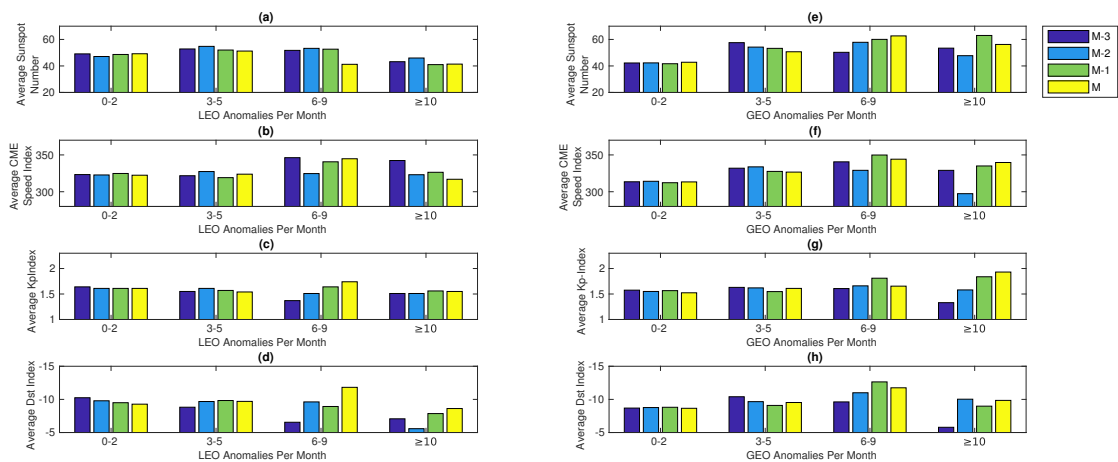
Figure 4. Relationship between LEO anomalies and the average SSN, Kp, CME speed, and Dst indices of the month the anomaly occurred and the previous three months, respectively (**a–d**). Relationship between GEO anomalies and the average SSN, Kp, CME speed, and Dst indices of the month the anomaly occurred and the previous three months, respectively (**e–h**). Note: M-1,2,3 indicate the months before the anomalous event, respectively.

In the analysis to assess the geomagnetic activity in Figure 4, the average Kp and Dst indices per month are computed by averaging all the samples within the month. However, this might result in a smoothing process that can hinder certain potential trends. Consequently, a different approach has been used to repeat the analysis by calculating the number of days in a month that exhibit a Kp-index ≥ 5 and Dst index ≤ -16 instead of average monthly values. These thresholds were defined considering that $\overline{Kp} = 1.6$, and $\overline{Dst} = -9.49$ during the study period. Accordingly, for GEO anomalies there are more average days with Kp-index ≥ 5 in those months with reported anomalies equal to or higher than 3 (Figure 5). The Kp-index surpasses 5 by an average day of 3.5 in the month of the event (M) and 3 for (M-1) and (M-2) for those months with $A_M \geq 10$. Similar trends are shown for those months where $6 \leq A_M \leq 9$, with the exception that there are more average days with notable geomagnetic activity in the previous month (M-1). Nevertheless, concerning the examination of LEO anomalies, no noteworthy patterns emerge, except for the months in which $6 \leq A_M \leq 9$.
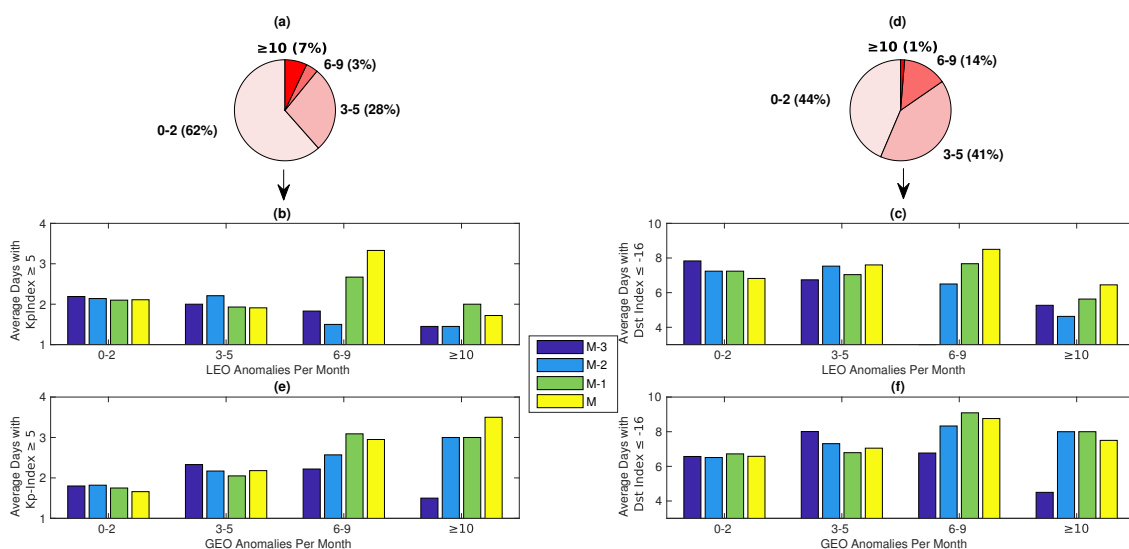

Figure 5. Relationship between LEO (**a–c**) and GEO (**d–f**) anomalies and number of days per month with Kp-index ≥ 5 and Dst index ≤ -16 of the month the anomaly occurred and the prior three months, respectively.

Seasonal Variations

In an attempt to determine any seasonal trends, Figure 6 illustrates the relationship between the average number of anomalies and the average SSN, Kp, CME speed, and Dst indices of a given month. For the GEO scenario, the anomaly rate increases significantly, but with a temporal delay (e.g., in November), as geomagnetic activity begins to rise in fall along with high solar activity.
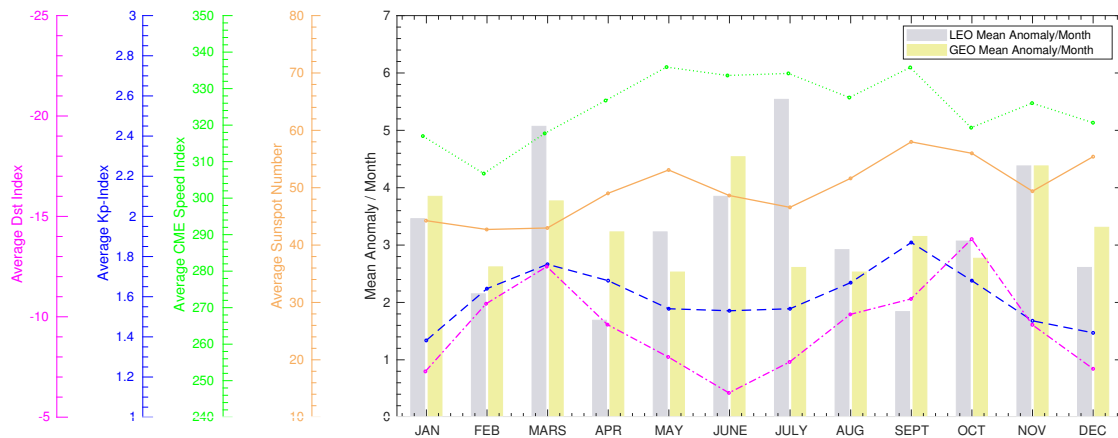

Figure 6. Monthly LEO/GEO anomaly rate correlation with the average SSN, Kp, CME speed, and Dst indices, computed for every month by averaging the 13 samples throughout the study period (2010–2022).

However, even in the absence of significant solar activity, the anomaly rate increases in the springtime due to an increase in geomagnetic activity (e.g., March). January and June are low magnetic activity months, yet they have significant anomaly rates. This, however, can be explained because of the SSN slight rise in December and a delay in the temporal reaction of the strong CME and SSN peaks recorded in May and June. These last cases deviate slightly from earlier findings from several studies, such as [10,12]. Indeed, after examining GEO anomalies throughout several periods, those studies concluded that GEO anomalies were less frequent in the summer and winter. Similar to GEO anomalies, LEO anomalies show a strong correlation with geomagnetic activity in spring and fall, which are the seasons in which aurora is at its most active around the equinoxes. As GEO, significant anomaly rates are also observed in summer times.

4.2. Daily Analysis

4.2.1. Solar and Magnetic Activity Assessment

In the monthly timescale analysis, it was noted that for some particular months the number of anomalies peaks in conjunction with some of the variables considered, notably for GEO anomalies (e.g., January 2014–April 2014). This suggests a rapid temporal response of satellite equipment due to some disturbances, such that a monthly examination might not be adequate to identify potential associations. Therefore, considering an average anomaly per day of 1.42 for LEO and 1.49 for GEO over the period (2010–2022), a daily analysis is proposed by selecting the days with three or more anomalies ($A_D \geq 3$). To avoid such days ($A_D \geq 3$) where disruptions from the same storms might be the source of their anomalies, days within the same month have been removed. For every selected day (event day) (see Table 1), and the six days before it, the daily average SSN, Kp, CME speed, and Dst indices are calculated and compared with their corresponding mean values.

The average SSN, Kp, CME speed, and Dst indices in the anomalous day occurrence and six days prior are shown in Figure 7. In the LEO scenario, geomagnetic indicators show average daily values that are even lower than the mean until the fourth prior day (D-4), when the magnetic perturbations typically surpass the mean. In terms of solar activity, it

is evident that during the 7 days under analysis, the average SSN consistently surpasses the mean, peaking on the third day before the anomalous occurrence. Since the CME speed index peaks on anomaly days (D), it is challenging to determine any relationship between the CMEs and anomalies on event days since the CME speed index has to exceed 1800 km/s in order to reach Earth in a single day [66]. Furthermore, it peaks three days before the event day, which is very consistent given that CMEs that have a linear velocity of 400–500 km/s need three to four days to reach Earth [67]. For instance, this could explain several recently reported anomalies such as that of FSSCat [68], of which one of the 6U CubeSats that composed it (^{3}Cat-5/A's mission) failed short after three months on a 535-km synchronous orbit with a 97.4° inclination. The FMPL-2 instrument of the ^{3}Cat-5/A's mission stopped communicating on 4 December 2020, just after the most powerful solar flare and coronal mass ejection observed during solar cycle 25 on 29 November 2020 [68]. Regarding GEO, the typical magnetic activity is higher than average from the first to the sixth day before any potential response, whereas the SSN remains moderately constant.

Table 1. Days selected to conduct the daily analysis that exhibited three or more anomalies.

| LEO (9 Days)	GEO (16 Days)	
15 July 2014	15 March 2010	15 October 2015
15 July 2017	30 June 2010	1 March 2016
6 May 2021	15 February 2011	12 June 2017
23 August 2021	15 March 2012	15 November 2017
21 November 2021	30 June 2012	15 May 2018
9 January 2022	15 November 2012	15 June 2018
15 August 2022	15 January 2013	5 November 2019
15 September-2022	15 January 2014	-
15 December 2022	30 June 2014	-
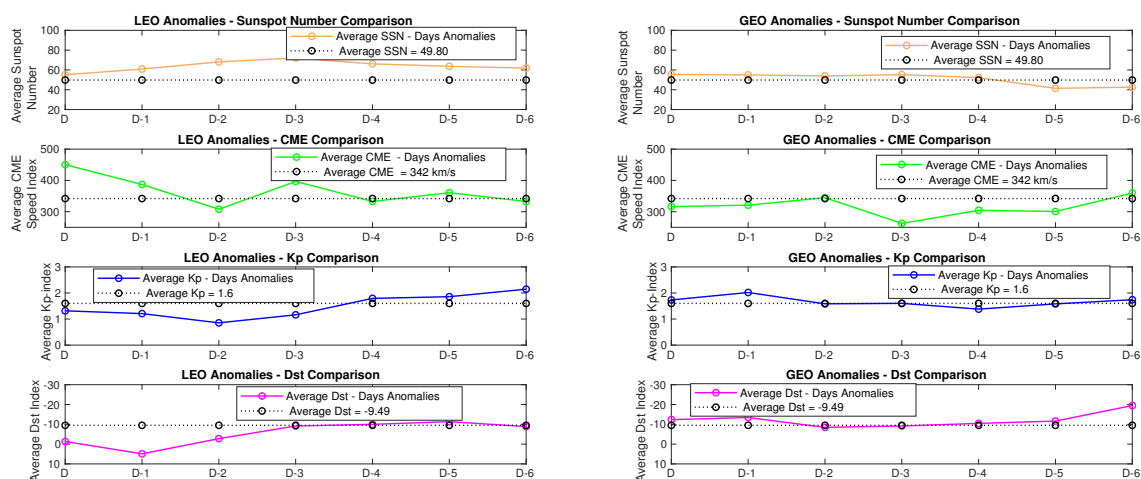
Figure 7. Assessment of solar and geomagnetic indicators during seven days (anomaly day + 6 prior days), for those days (anomaly day, D) with LEO and GEO anomalies ≥ 3.

4.2.2. Particles Flux Density Assessment

Aside from the potential radiation effects during geomagnetic storms and solar activity fluctuations, examining particle density and distribution around Earth is critical to understanding the causes and frequency of satellite anomalies. Thus, protons, electrons, and X-ray fluxes were compared for days with high and low anomaly rates (see Figure 8).

Several conclusions can be extracted from Figure 8. Firstly, for LEO and GEO, days with anomalies show a significant increase in proton flux as compared to days without anomalies. This tendency is not limited to the anomalous day (D), but extends throughout the six days preceding the event day. For LEO, this increment, which is notably larger than for GEO, tends to be maximum on the anomalous day (D), and the day before (D-1), whereas for GEO tends to be at the fifth and sixth days (D-5 and D-6). These outcomes point out that GEO and LEO anomalies are potentially caused by solar proton events and trapped protons (e.g., inner Van Allen belt). In terms of electron flux, in the GEO scenario, those days with anomalies had a higher average electron flux than those without, not only on the anomaly day but over the entire 7-day span. Nonetheless, for the LEO scenario, and in contrast to what is expected, days with no reported failures had a higher electron flux than days with $A_D \geq 3$, not just on the event day, but throughout the 7-day window. Regarding X-ray concentrations, the days presenting LEO anomalies as well as the six days before the anomaly showed larger X-ray particles than the non-anomaly days selected, however, those patterns are not observed for GEO anomalies.
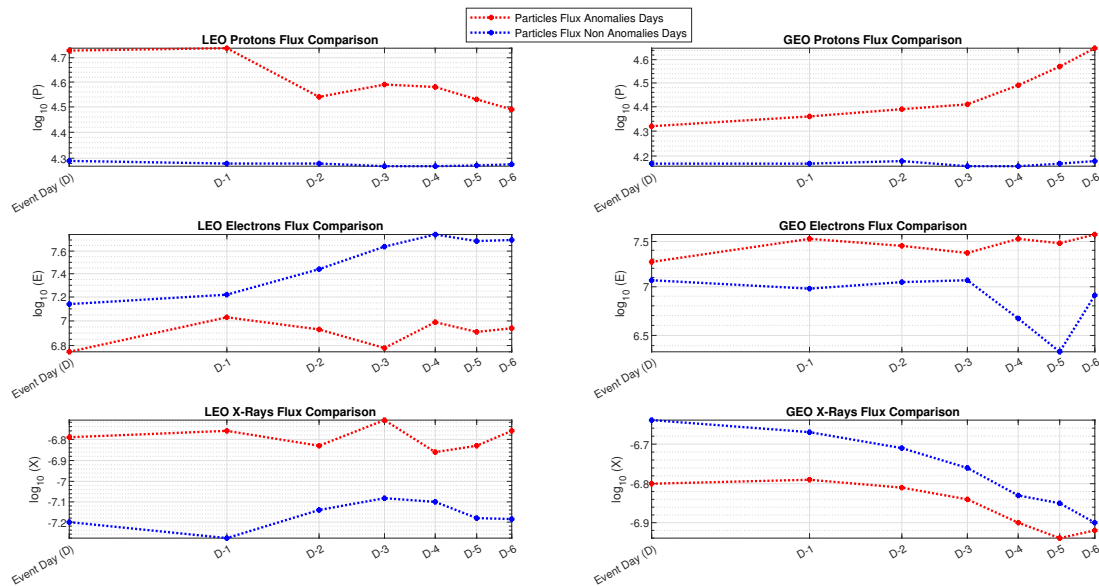

Figure 8. Proton, electron, and X-ray flux time series comparison between days with no reported anomalies (see Table 2) and those selected days with $A_D \geq 3$ during a seven-day window (see Table 1). Given that one or a few days can have significantly higher particle concentrations than others, logarithmic charts are employed to respond to the large value ranges. Before the log() application, proton (P), electron (E), and X-ray flux (X) were in protons/(cm·day·sr), electrons/(cm·day·sr), and W/m^2, respectively.

Table 2. Days with no reported anomalies selected to compare their average particle flux with those days with $A_D \geq 3$.

LEO (6 Days)	GEO (6 Days)
15 July 2014	15 October 2015
15 July 2017	1 March 2016
6 May 2021	12 June 2017
23 August 2021	15 November 2017
21 November 2021	15 May 2018
9 January 2022	15 June 2018

4.3. Orbit Inclination's Impact on Anomaly Rate

The Earth's magnetic field traps protons and electrons, resulting in radiation belts known as Van Allen belts. Thus, as mentioned before, the radiation density that satellites must cross during their course is significantly influenced by their orbital altitude and inclination. As for orbit altitude, by which the analysis has been simplified by categorizing LEO and GEO satellites, each satellite whose reported anomalies have been considered in this study has had its orbital inclination classified as seen in Figure 9. Regarding LEO, those active satellites whose orbital inclination (θ) were within 15°–30° and 45°–60° ranges presented slightly higher anomaly rate percentages than other ranges such as 0°–15° and 75°–90°, whereas active satellites orbiting between 60°–75° range presented the higher anomaly rate (22.5%). Unlike the unexpectedly high failure rate presented in the 15°–30° range, the rates at 45°–60° and 60°–75° are highly consistent considering that higher electron concentrations are observed between 45° and 85°, while for low inclination orbits ($\theta \leq 30°$), the electron concentrations are relatively low [69]. The high anomaly rate of those satellites whose inclination ranges between 45° and 60° can also be directly linked with the several passes per day through the SAA, situated at 200–800 km over the Earth's surface [70]. Furthermore, as indicated in Figure 9, polar and near-polar orbits ($90° \leq \theta < 105°$) also present moderately high anomaly rates, which is consistent considering that polar-orbiting satellites pass through dangerous charged particle concentrations (e.g., electrons of energy about 1 MeV) several times per day [71]. In addition, with the open magnetic field lines over the poles, polar-orbiting satellites are exposed directly to large solar proton fluxes and lower energy GCR [72]. As for geosynchronous orbit, considering the operational benefits when $\theta = 0°$ (geostationary orbit), 76% of the active satellites from 2010 to 2022 had an orbit inclination within 0° and 15° [38]. Accordingly, 94.1% of those satellites whose anomalies have been incorporated into the analysis have an orbit inclination between 0° and 15°. As a result, having data concentrated in a single orbit inclination range presents significant challenges when exploring the GEO orbit inclination relationship with satellite anomaly rate. Hence, as depicted in Figure 9, for those GEO active satellites within 0° and 15°, 64% (304 satellites) have experienced an anomaly during the period of study, whereas within 30° and 45°, 57% (4 satellites) failed partially or totally.
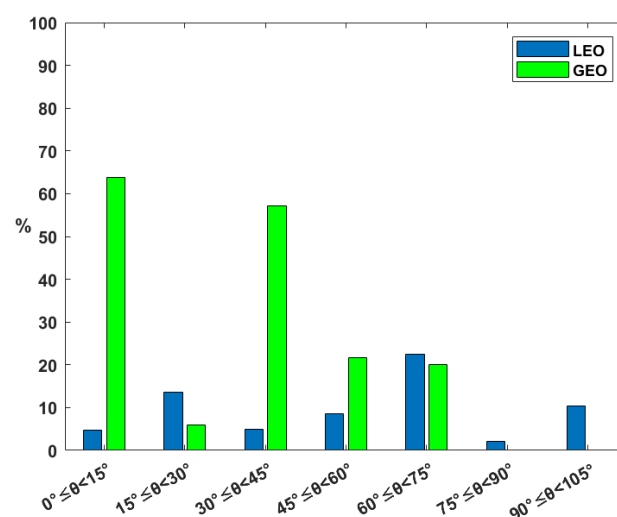

Figure 9. Orbital inclination classification for LEO and GEO satellites whose anomalies were selected for the analysis. The satellites failures percentage in each orbit inclination range is normalized by dividing the total number of satellites failed by active satellites in that range from 2010 to 2022 according to Seradata [38].

5. Discussion and Conclusions

This study has examined the relationship between space weather and anomalies observed in LEO and GEO satellites, with a particular emphasis on solar and geomagnetic

activity. The analysis outcomes confirm that solar activity is critical for satellite anomalies. However, as opposed to what is generally thought, the anomaly rate increases do not necessarily coincide with periods of high solar activity. However, this is consistent considering that during periods of low sunspot number, cosmic ray particles penetrate the inner solar system, and the density of relativistic electrons increases significantly. In addition, this suggests that alongside the assessment of solar flares and CMEs emission of radiation fluxes reaching Earth's surroundings, the distribution of those particles in GEO and LEO, and how they are trapped by the Earth's magnetic field (Van Allen belts, SAA) also play a fundamental role.

LEO satellites highlight that high solar activity correlates with a rise in anomaly reports, particularly during specific months tied to heightened sunspot activity and CMEs. On the other hand, when monthly averaged statistics were evaluated, no significant trends regarding geomagnetic disturbances and storms were found, which might be due to the high shielding effects of the magnetic field in comparison with GEO orbit. Conversely, for GEO anomalies, generally, those months with high anomaly rates are associated significantly with high geomagnetic activity, whereas for solar activity, important patterns are observed only in a monthly timescale. In a daily timescale, only those days with high LEO anomalies present a high solar activity alongside a significant magnetic disturbance during the six days before, whereas, for GEO, the SSN remains close to the mean during the days before. According to these findings, radiation effects often take effect on LEO more rapidly than on GEO satellites.

When examining the association between different particle concentrations and anomaly occurrence, for LEO and GEO, the days with reported anomalies ($A_D \geq 3$) presented larger proton flux than those selected days with no reported failures not even on the day of the event, but during the week before it. Given that the majority of the investigated LEO satellites have orbital inclinations ranging from 45° to 75° and 90° to 105°, this suggests that LEO anomalies may be caused by trapped proton concentrations in the SAA region and solar activity fluctuations reaching the Earth's poles. Furthermore, for GEO, days with $A_D \geq 3$ showed higher electron flux than days with $A_D = 0$ throughout the seven days, whereas, for LEO, days with $A_D \geq 3$ presented larger X-ray concentrations than days with $A_D = 0$ during the complete time window analyzed.

Besides the environmental effects, it is crucial to emphasize specific influencing factors, such as the radiation tolerance of satellite materials and components, along with certain orbital characteristics. Certain materials and designs may enhance resilience, while others leave systems particularly vulnerable to damaging radiation events. Moreover, environmental conditions, especially orbital characteristics like inclination and altitude, play a crucial role as they influence the degree of radiation exposure, particularly from energetic particles captured in the Earth's magnetic field. The correlations obtained from this analysis may aid in defining operational strategies (e.g., by switching off some vulnerable systems, and reserve mode, among others) to minimize radiation effects on satellite systems. However, detailed disclosure and availability of satellite anomaly data are essential to assess the effectiveness of those mitigation strategies and advance toward their innovation. Furthermore, providing a detailed specification of the types of anomalies, including the affected components and their possible causes, will greatly enhance the analysis and categorization of the vulnerability of various satellite equipment. Future research should delve deeper into several directions. On one hand, it is decisive to advance in monitoring, characterizing, and predicting radiation levels by using, for instance, physics-based, machine-learning models, and real-time satellite observations. On the other hand, it is crucial to investigate novel alternative radiation-hardened and tolerant systems and to assess the robustness of satellite materials.

Data Availability Statement: Data are contained within the article.

Conflicts of Interest: The authors declare that they have no known competing financial interests or personal relationships that could have appeared to influence the work reported in this paper.

Abbreviations

The following abbreviations are used in this manuscript:

A	Number of Anomalies
A_D	Number of Anomalies per Day
A_M	Number of Anomalies per Month
ADCS	Attitude Determination Control System
BA	Brightness Asymmetry
CMEs	Coronal Mass Ejections
COMMS	Communication System
CPA	Central Position Angle
Dst	Disturbance Storm Time
EPS	Electrical Power System
ESA	European Space Agency
ESD	Electrostatic Discharge
FMPL-2	Flexible Microwave Payload—Version 2
FOV	Field of View
GCR	Galactic Cosmic Rays
GEO	Geosynchronous Orbit
LASCO	Large Angle and Spectrometric Coronagraph
LEO	Low Earth Orbit
NASA	National Aeronautics and Space Administration
NOAA	National Oceanic and Atmospheric Administration
OA	Outline Asymmetry
OBC	On-Board Computer
RadHard	Radiation Hardened
SAA	South Atlantic Anomaly
SEB	Single Event Burnout
SEL	Single Event Latch-up
SEU	Single Event Upset
SOHO	Solar and Heliospheric Observatory Satellite
SPEs	Solar Particle Events
SSN	Sunspot Number
TD	Total Dose
TT&C	Telemetry, Tracking, and Command
UV	Ultraviolet

References

1. Telastra Inc. Public Record Satellite Anomaly Database (PRSADB). 2021. Communications Satellite Databases. Available online: https://scholar.google.com/scholar_lookup?title=Communications%20satellite%20databases&publication_year=2021&author=N.H.%20Telastra%20Inc.Public%20Record%20Satellite%20Anomaly%20Database%20(PRSADB) (accessed on 2 February 2022).

2. Jacklin, S.A. Small-Satellite Mission Failure Rates. 2019. Available online: https://ntrs.nasa.gov/api/citations/20190002705/downloads/20190002705.pdf (accessed on 11 July 2024).

3. Quan, L.; Wang, D.; Zhang, Q.; Zhang, S.; Li, L.; Wang, S.; Jing, T.; Meng, Y.; Liu, Y.; Tian, C. Radiation environment and effect detection based on global navigation constellation. *Open Astron.* **2023**, *32*, 20220204. [CrossRef]

4. Venkatesan, A.; Lowenthal, J.; Prem, P.; Vidaurri, M. The impact of satellite constellations on space as an ancestral global commons. *Nat. Astron.* **2020**, *4*, 1043–1048. [CrossRef]

5. Novak, J.; Hastings, D. Analysis of proliferated low Earth orbit constellation resilience against solar weather radiation effects. *Acta Astronaut.* **2023**, *202*, 292–302. [CrossRef]

6. Ecoffet, R. Overview of in-orbit radiation induced spacecraft anomalies. *IEEE Trans. Nucl. Sci.* **2013**, *60*, 1791–1815. [CrossRef]

7. Mullen, E. *Space Radiation Environments for Parts Selection/Test Considerations in Typical Satellite Orbits*; Tech. Rep.; Assurance Technology Corporation: Carlisle, MA, USA, 2003; Volume 1.

8. Tribble, A.C. *The Space Environment: Implications for Spacecraft Design-revised and Expanded Edition*; Princeton University Press: Princeton, NJ, USA, 2020.

9. Purvis, C.K.; Garrett, H.B.; Whittlesey, A.C.; Stevens, N.J. *Design Guidelines for Assessing and Controlling Spacecraft Charging Effects*; National Aeronautics and Space Administration: Washington, DC, USA, 1984.

10. Jia, X.; Liu, J.; Zhang, X. The Analysis of Ionospheric TEC Anomalies Prior to the Jiuzhaigou Ms7.0 Earthquake Based on BeiDou GEO Satellite Data. *Remote Sens.* **2024**, *16*, 660 [CrossRef]

11. Iucci, N.; Levitin, A.E.; Belov, A.V.; Eroshenko, E.A.; Ptitsyna, N.G.; Villoresi, G.; Chizhenkov, G.V.; Dorman, L.I.; Gromova, L.I.; Parisi, M.; et al. Space weather conditions and spacecraft anomalies in different orbits. *Space Weather* **2005**, *3*, 16 [CrossRef]

12. Choi, H.-S.; Lee, J.; Cho, K.-S.; Kwak, Y.-S.; Cho, I.-H.; Park, Y.-D.; Kim, Y.-H.; Baker, D.N.; Reeves, G.D.; Lee, D.-K. Analysis of GEO spacecraft anomalies: Space weather relationships. *Space Weather* **2011**, *9*, S06001. [CrossRef]

13. Pilipenko, V.; Yagova, N.; Romanova, N.; Allen, J. Statistical relationships between satellite anomalies at geostationary orbit and high-energy particles. *Adv. Space Res.* **2006**, *37*, 1192–1205. [CrossRef]

14. Paladini, S. *The New Frontiers of Space*; Springer: Berlin/Heidelberg, Germany, 2019.

15. Foreman Campins, L. *NewSpace and the European Space Economy*. Master's Thesis, Universitat Politècnica de Catalunya, Barcelona, Spain, 2023.

16. Cloitre, A.; Dos Santos Paulino, V.; Theodoraki, C. The quadruple/quintuple helix model in entrepreneurial ecosystems: An institutional perspective on the space case study. *R&D Manag.* **2023**, *53*, 675–694.

17. Mertens, C.J.; Kress, B.T.; Wiltberger, M.; Tobiska, W.K.; Grajewski, B.; Xu, X. *Atmospheric Ionizing Radiation from Galactic and Solar Cosmic Rays*; InTech Open Access Publisher: Rijeka, Croatia, 2012.

18. Serrano Gonçalves, P.C. *The Ionising Radiation Environment in the Solar System*. 2021. Available online: https://pages.lip.pt/space/wp-content/uploads/sites/9/2023/02/The-Ionising-Radiation-Environment-in-the-Solar-System-Lesson.pdf (accessed on 2 February 2022).

19. Miroshnichenko, L. Energetic Particles in the Geosphere. In *Solar-Terrestrial Relations: From Solar Activity to Heliobiology*; Springer: Berlin/Heidelberg, Germany, 2023; pp. 123–148.

20. Miroshnichenko, L.I. Solar cosmic rays: 75 years of research. *Phys. Uspekhi* **2018**, *61*, 323. [CrossRef]

21. Xu, J.; Guo, M.; Lu, M.; He, H.; Yang, G.; Xu, J. Effect of Alpha-Particle Irradiation on InGaP/GaAs/Ge Triple-Junction Solar Cells. *Materials* **2018**, *11*, 944. [CrossRef] [PubMed]

22. Waets, A.; Bilko, K.; Coronetti, A.; Emriskova, N.; Barbero, M.S.; Alia, R.G.; Durante, M.; Schuy, C.; Wagner, T.; Esposito, L.S.; et al. Very-High-Energy Heavy Ion Beam Dosimetry using Solid State Detectors for Electronics Testing. *IEEE Trans. Nucl. Sci.* **2024**, *71*, 1837–1845. [CrossRef]

23. Lu, Y.; Shao, Q.; Yue, H.; Yang, F. A review of the space environment effects on spacecraft in different orbits. *IEEE Access* **2019**, *7*, 93473–93488. [CrossRef]

24. Barth, J.L Space and atmospheric environments: From low earth orbits to deep space. In *Protection of Materials and Structures from Space Environment: ICPMSE-6*; Springer: Berlin/Heidelberg, Germany, 2004; pp. 7–29.

25. Ya'acob, N.; Zainudin, A.; Magdugal, R.; Naim, N.F. Mitigation of space radiation effects on satellites at Low Earth Orbit (LEO). In Proceedings of the 6th IEEE International Conference on Control System, Computing and Engineering ICCSCE2016, Penang, Malaysia, 25–27 June 2016; pp. 56–61.

26. Baker, D.N.; Erickson, P.J.; Fennell, J.F.; Foster, J.C.; Jaynes, A.N.; Verronen, P.T. Space Weather Effects in the Earth's Radiation Belts. *Space Sci. Rev.* **2018**, *214*, 17. [CrossRef]

27. McMurchie, E.J. Quantifying Radiation Effects of Energetic Electron Precipitation from the Van Allen Radiation Belts into the Earth's Atmosphere. Master's Thesis, University of Colorado at Boulder, Boulder, CO, USA, 2022.

28. Bolin, J.A. Comparative Analysis of Selected Radiation Effects in Medium Earth Orbits. Ph.D. Thesis, Naval Postgraduate School, Monterey, CA, USA, 1997.

29. Baker, D.N. Satellite anomalies due to space storms: The effects of space weather on spacecraft systems and subsystems; *Space Storms and Space Weather Hazards*; Springer: Berlin/Heidelberg, Germany, 2001; pp. 285–311.

30. Garrett, H.B.; Close, S. Impact-induced ESD and EMI/EMP effects on spacecraft—A review. *IEEE Trans. Plasma Sci.* **2013**, *41*, 3545–3557. [CrossRef]

31. Jun, I.; Garrett, H.; Kim, W.; Zheng, Y.; Fung, S.F.; Corti, C.; Ganushkina, N.; Guo, J. A review on radiation environment pathways to impacts: Radiation effects, relevant empirical environment models, and future needs. *Adv. Space Res.* **2024**. ISSN 0273-1177. [CrossRef]

32. Nwankwo, V.U.J.; Jibiri, N.N.; Kio, M.T. The Impact of Space Radiation Environment on Satellites Operation in Near-Earth Space. In *Satellites Missions and Technologies for Geosciences*; IntechOpen: London, UK, 2020; Volume 1, pp. 73–90.

33. Johnson, R.E.; Carlson, R.W.; Cooper, J.F.; Paranicas, C.; Moore, M.H.; Wong, M.C.Radiation effects on the surfaces of the Galilean satellites. In *Jupiter: The Planet, Satellites and Magnetosphere*; Cambridge University Press: Cambridge, UK, 2004; Volume 1, pp. 485–512.

34. Qiu, F.; Gong, J.; Tong, G.; Han, S.; Zhuang, X.; Zhu, X. Near-infrared Light-Induced Polymerizations: Mechanisms and Applications. *ChemPlusChem* **2024**, *89*, e202300782. [CrossRef]

35. Likar, J.J.; Bogorad, A.; August, K.A.; Lombardi, R.E.; Kannenberg, K.; Herschitz, R. Spacecraft Charging, Plume Interactions, and Space Radiation Design Considerations for All-Electric GEO Satellite Missions. *IEEE Trans. Plasma Sci.* **2015**, *43*, 3099–3108. [CrossRef]

36. Schwadron, N.A.; Cooper, J.F.; Desai, M.; Downs, C.; Gorby, M.; Jordan, A.P.; Joyce, C.J.; Kozarev, K.; Linker, J.A.; Mikíc, Z.; et al. Particle Radiation Sources, Propagation and Interactions in Deep Space, at Earth, the Moon, Mars, and Beyond: Examples of Radiation Interactions and Effects. *Space Sci. Rev.* **2017**, *212*, 1069–1106. [CrossRef]

37. Fortescue, P.; Swinerd, G.; Stark, J. *Spacecraft Systems Engineering*; John Wiley & Sons: Hoboken, NJ, USA, 2011.

38. SpaceTrack. SpaceTrack database: Number of Spacecraft's Launches 2010–2023. Available online: https://spacetrak.seradata.com/Queries (accessed on 1 April 2024).

39. Agency European Space. EO PORTAL. Available online: https://www.eoportal.org/ (accessed on 30 November 2022).

40. National Aeronautics and Space Administration. Small Satellites Mission Failures Rate [Online]. Available online: https://ntrs.nasa.gov/citations/20190002705 (accessed on 12 December 2022).

41. Buitrago-Leiva, J.N.; El Khayati Ramouz, M.; Camps, A.; Ruiz-de-Azua, J.A. Towards a second life for Zombie Satellites: Anomaly occurrence and potential recycling assessment. *Acta Astronaut.* **2024**, *217*, 238–245 [CrossRef]

42. Zheng, Y.; Ganushkina, N.Y.; Jiggens, P.; Jun, I.; Meier, M.; Minow, J.I.; O'Brien, T.P.; Pitchford, D.; Shprits, Y.; Tobiska, W.K.; et al. Space Radiation and Plasma Effects on Satellites and Aviation: Quantities and Metrics for Tracking Performance of Space Weather Environment Models. *Space Weather* **2019**, *17*, 1384–1403. [CrossRef] [PubMed]

43. Stassinopoulos, E.; Brucker, G.; Adolphsen, J.; Barth, J. Radiation-induced anomalies in satellites. *J. Spacecr. Rocket.* **1996**, *33*, 877–882. [CrossRef]

44. NASA. Solar Activity. Available online: https://spaceplace.nasa.gov/solar-activity/en/ (accessed on 23 April 2024).

45. Royal Observatory of Belgium. 2024. Available online: http://www.sidc.be/silso/home (accessed on 12 April 2024).

46. NOAA National Centers for Environmental Information. Kp and Ap indices. 2024. Available online: https://www.ngdc.noaa.gov/geomag/indices/kp_ap.html (accessed on 12 April 2024).

47. Bryant, K.; Young, R.P.; LeFevre, H.J.; Kuranz, C.C.; Olson, J.R.; McCollam, K.J.; Forest, C.B. Creating and studying a scaled interplanetary coronal mass ejection. *Phys. Plasmas* **2024**, *31*, 042901. [CrossRef]

48. Jain, S.; Podladchikova, T.; Chikunova, G.; Dissauer, K.; Veronig, A.M. Coronal dimmings as indicators of the direction of early coronal mass ejection propagation. *Astron. Astrophys.* **2024**, *683*, A15.

49. Singh, R.; Powar, V. The Future of Generation, Transmission, and Distribution of Electricity. In *The Advancing World of Applied Electromagnetics: In Honor and Appreciation of Magdy Fahmy Iskander*; Springer: Berlin/Heidelberg, Germany, 2024; pp. 349–383.

50. NASA.SOHO LASCO CME CATALOG—Version 2. Available online: https://cdaw.gsfc.nasa.gov/CME_list/UNIVERSAL_ver2/1996_01/univ1996_01.html (accessed on 2 February 2024).

51. Solanki, S.K.; Teriaca, L.; Barthol, P.; Curdt, W.; Inhester, B. European Solar Physics: Moving from SOHO to Solar Orbiter and Beyond. *Mem. Soc. Astron. Ital.* **2013**, *84*, 286.

52. Kilcik, A.; Yurchyshyn, V.B.; Abramenko, V.; Goode, P.R.; Gopalswamy, N.; Ozguc, A.; Rozelot, J.P. Maximum Coronal Mass Ejection Speed as an Indicator of Solar and Geomagnetic Activities. *Astrophys. J.* **2011**, *727*, 44. [CrossRef]

53. Welling, D.T. The long-term effects of space weather on satellite operations. *Ann. Geophys.* **2010**, *28*, 1361–1367. [CrossRef]

54. Tacza, J.; Li, G.; Raulin, J-.P. Effects of Forbush Decreases on the global electric circuit. *Space Weather* **2024**, *22*, e2023SW003852. [CrossRef]

55. Banerjee, A.; Bej, A.; Chatterjee, T.N. On the existence of a long range correlation in the geomagnetic disturbance storm time (Dst) index. *Astrophys. Space Sci.* **2012**, *337*, 23–32. [CrossRef]

56. Dachev, T.P. South-Atlantic Anomaly magnetic storms effects as observed outside the International Space Station in 2008–2016. *J. Atmos. Sol. Terr. Phys.* **2018**, *179*, 251–260. [CrossRef]

57. Kyoto University. Dst Provisional Values. Available online: https://wdc.kugi.kyoto-u.ac.jp/dst_provisional/index.html (accessed on 1 February 2024).

58. Filippov, B.P. Mass ejections from the solar atmosphere. *Phys. Uspekhi* **2019**, *62*, 847. [CrossRef]

59. Boenig, H. *Plasma Science and Technology*; Cornell University Press: Ithaca, NY, USA, 2019.

60. Space Weather Prediction Center, National Oceanic and Atmospheric Administration. GOES Electron Flux. 2024. Available online: https://www.swpc.noaa.gov/products/goes-electron-flux (accessed on 10 April 2024).

61. Space Weather Prediction Center, National Oceanic and Atmospheric Administration. GOES Proton Flux. 2024. Available online: https://www.swpc.noaa.gov/products/goes-proton-flux (accessed on 10 April 2024).

62. Höeffgen, S.K.; Metzger, S.; Steffens, M. Investigating the effects of cosmic rays on space electronics. *Front. Phys.* **2020**, *8*, 318. [CrossRef]

63. Ziemacki, T.; Drzazga, R. The impact of radiation on electronics in space: A review. *Acta Astronaut.* **2019**, *157*, 172–179. [CrossRef]

64. The Bureau of Meteorology. Australian Space Weather Forecasting Centre. Meaning of X-Ray Fluxes From the Sun. 2024. Available online: https://www.sws.bom.gov.au/Educational/2/1/3 (accessed on 10 April 2024).

65. Miteva, R.; Samwel, S.W.; Tkatchova, S. Space weather effects on satellites. *Astronomy* **2023**, *2*, 165–179. [CrossRef]

66. Nirmal Kumar, R.; Ranjith Dev Inbaseelan, C.; Karthikeyan, E.; Nithyasree, M.; Johnson Jeyakumar, H. Analysis of solar energetic particle (SEP) event on the geomagnetic environment during 24th solar cycle. *Astrophys. Space Sci.* **2024**, *369*, 56.

67. Rodriguez, L.; Shukhobodskaia, D.; Niemela, A.; Maharana, A.; Samara, E.; Verbeke, C.; Magdalenic, J.; Vansintjan, R.; Mierla, M.; Scolini, C.; et al. Validation of EUHFORIA cone and spheromak Coronal Mass Ejection Models. *arXiv* **2024**, arXiv:2405.04637. [CrossRef]

68. Camps, A.; Munoz-Martin, J.F.; Ruiz-de-Azua, J.A.; Fernandez, L.; Perez-Portero, A.; Llaveria, D.; Herbert, C.; Pablos, M.; Golkar, A.; Gutiérrez, A.; et al. FSSCat: The Federated Satellite Systems 3 Cat Mission: Demonstrating the capabilities of CubeSats to monitor essential climate variables of the water cycle [Instruments and Missions]. *IEEE Geosci. Remote Sens. Mag.* **2022**, *10*, 260–269. [CrossRef]

69. NASA. NASA Lesson: Solar Flares and Their Effect on Earth's Magnetosphere. 2024. Available online: https://llis.nasa.gov/lesson/824 (accessed on 12 May 2024).

70. Nasuddin, K.A.; Abdullah, M.; Abdul Hamid, N.S. Characterization of the South Atlantic Anomaly. *Nonlinear Process. Geophys.* **2019**, *26*, 25–35. [CrossRef]

71. Velazco, R.; Fouillat, P.; Reis, R. *Radiation Effects on Embedded Systems*; Springer: Dordrecht, The Netherlands, 2007.

72. Samwel, S.W.; El-Aziz, E.A.; Garrett, H.B.; Hady, A.A.; Ibrahim, M.; Amin, M.Y. Space radiation impact on smallsats during maximum and minimum solar activity. *Adv. Space Res.* **2019**, *64*, 239–251. [CrossRef]